Published in final edited form as:

Nanomedicine (Lond). 2015 June ; 10(11): 1775–1784. doi:10.2217/nnm.15.27.

Delivery of siRNA to ovarian cancer cells using laser-activated carbon nanoparticles

Aritra Sengupta[1,‡], **Roman Mezencev**[2,‡], **John F McDonald**[2], and **Mark R Prausnitz**[1,*]

[1]School of Chemical & Biomolecular Engineering, Georgia Institute of Technology, Atlanta, GA 30332, USA

[2]School of Biology, Georgia Institute of Technology, Atlanta, GA 30332, USA

Abstract

Aim—The RNAi-mediated knockdown of gene expression is an attractive tool for research and therapeutic purposes but its implementation is challenging. Here we report on a new method based on photoacoustic delivery of siRNA developed to address some of these challenges.

Materials & methods—Physical properties and photoacoustic emission of carbon black (CB) particles upon near-infrared laser irradiation were characterized. Next, ovarian cancer cells Hey A8-F8 were exposed to near-infrared nanosecond laser pulses in the presence of siRNA targeting *EGFR* gene and CB particles. The intracellular delivery of siRNA and silencing of the target gene were determined by specific qPCR assays.

Results & conclusion—Laser-activated CB nanoparticles generated photoacoustic emission and enabled intracellular delivery of siRNA and significant knockdown of its target *EGFR* mRNA. This physical method represents a new promising approach to targeted therapeutic delivery of siRNA.

Keywords

EGFR; intracellular delivery; nanosecond laser; photoacoustics; siRNA

Since the discovery of siRNA-mediated gene knockdown in *Caenorhabditis elegans* [1] and its subsequent implementation in mammalian cells [2], this method has gained considerable attention because it has the potential to knock down any specific gene in the body and

*Author for correspondence: prausnitz@gatech.edu.
‡Authors contributed equally

Ethical conduct of research

The authors state that they have obtained appropriate institutional review board approval or have followed the principles outlined in the Declaration of Helsinki for all human or animal experimental investigations. In addition, for investigations involving human subjects, informed consent has been obtained from the participants involved.

Financial & competing interests disclosure

This work was carried out in the Center for Drug Design, Development and Delivery and the Institute for Bioengineering and Bioscience at Georgia Tech, and was supported in part by the NIH and The Shurl & Kay Curci Foundation. The authors have no other relevant affiliations or financial involvement with any organization or entity with a financial interest in or financial conflict with the subject matter or materials discussed in the manuscript apart from those disclosed.

No writing assistance was utilized in the production of this manuscript.

specifically modulate more therapeutic targets than typical small-molecule drugs [3]. Using this RNAi approach, *in vitro* and *in vivo* studies have already demonstrated therapeutic potential of siRNA-mediated gene knockdown in diseases like hypercholesterolemia [4], liver cirrhosis [5], hepatitis B virus infection [6,7], human papilloma-virus infection [8] and bone cancer [9]. Human clinical trials are also underway [10,11]. However, a key challenge to clinical translation is delivering siRNA into cells, because siRNA molecules are big (~13 kDa), heavily negatively charged and subject to rapid renal clearance and degradation by endogenous enzymes *in vivo* [3,12].

Most of the current techniques to deliver siRNA involve the use of viral vectors [13,14], lipid vesicles [15,16], solid nanoparticle formulations [17–19] or hydrodynamic injections [20]. Viral methods suffer from drawbacks like cytotoxicity, insertional mutagenesis and activation of immune response [21,22]. A major hurdle in nonviral delivery is avoiding endosomal degradation and achieving endosomal escape of siRNA [23–25]. Another approach is to directly deliver siRNA into cytoplasm, which avoids the endocytic pathway completely. Examples of such methods are electroporation, ultrasound-induced poration, microinjection, etc. A common challenge with these methods is to maintain high viability of transfected cells under conditions associated with high intracellular uptake [26].

In this study, we propose a method that uses laser-irradiated carbon black (CB) nanoparticles to achieve intracellular delivery of siRNA. In this method, we expose CB nanoparticles to nanosecond pulsed laser, causing the nanoparticles to preferentially heat up, which results in particle expansion [27], liquid vaporization [27,28] and/or chemical reaction ($C[s] + H_2O[l] \rightarrow CO[g] + H_2[g]$) [29], followed by generation of acoustic waves, leading to poration of cell membranes [30,31]. Molecules then passively transport into the cell without the need of endocytosis. Previously we demonstrated this method to be efficient in delivering small molecules like calcein and larger proteins like bovine serum albumin [30,31]; here we seek to extend the application to siRNA not only to show intracellular uptake of siRNA, but to demonstrate RNA interference by knocking down expression of a specific gene by delivery of biologically active siRNA.

This method of intracellular delivery does not involve internalization of the CB nanoparticles, unlike other methods of intracellular delivery based on laser-particle interactions [32]. In our approach, the nanoparticles transduce laser energy (i.e., photons) into mechanical energy (i.e., acoustic waves) that impact the cell membrane to increase its permeability [31]. In this way, siRNA provided in the extracellular medium can then diffuse directly into its area of target, in other words, cytoplasm, where the mature mRNAs are present. For this reason, we believe the siRNA delivery to the cytoplasm is especially well suited to delivery by laser-activated CB nanoparticles, as opposed to, for example, DNA, which typically has an intranuclear target for transfection.

We carried out this study in ovarian cancer cells in anticipation of future applications to treat ovarian cancer. Ovarian cancer is the most lethal of all gynecological cancers and the fifth leading cause of cancer-related deaths in women in the USA [33]. According to the US National Cancer Institute, in 2014 there will be almost 22,000 new cases of ovarian cancer and more than 14,000 women will die of this disease nationally [34]. Current treatment of

advanced ovarian cancer, which includes debulking surgery and platinum-based chemotherapy, is initially effective in the majority of patients; however, most of them eventually develop disease recurrence [35].

We have previously shown that targeting *EGF* receptor (*EGFR*) by siRNA-mediated gene knockdown increased sensitivity of ovarian cancer cells to a traditional anticancer agent docetaxel [36]. This suggests that *EGFR* can serve as a viable target for development of siRNA-based therapies of ovarian cancer.

In this study, we first tested the hypothesis that laser-activated CB nanoparticles cause enhanced uptake of FITC-dextran (70 kDa) by ovarian cancer cells and then demonstrated uptake of anti-*EGFR* siRNA into ovarian cancer cells and knockdown of its target *EGFR* mRNA.

Delivery system design

The long-term goal of this study is to introduce nanoparticles into a tissue, and irradiate the tissue with laser in order to heat the CB nanoparticles selectively through absorption of the laser energy by the nanoparticles. This causes CB nanoparticles to generate acoustic emissions leading to intracellular delivery of siRNA into ovarian cancer cells.

Given this goal, we chose to irradiate the CB nanoparticles with a 1064-nm wavelength near-infrared (NIR) laser because light at this wavelength can be generated using relatively inexpensive commercial lasers and is poorly absorbed by biological tissues [37], thereby enabling deeper penetration in tissues [38]. We chose CB nanoparticles as the photoacoustic transducers because they absorb IR light efficiently (Supplementary Figure 1, see online at www.future-medicine.com/doi/full/10.2217/NNM.15.27) [39], can be of suitable size for injection and enhanced permeation and retention effects [40], have been shown to generate photoacoustic emissions [29] and were found to be nontoxic to cells in a previous study at concentrations useful for intracellular delivery [31].

To make CB nanoparticle suspensions, commercial CB powder was dispersed in an aqueous solution of Tween 80, a nonionic surfactant, using a needle sonicator for 15 min at a final concentration of 400 mg/l (see Supplementary Materials & Methods). Dynamic light scattering showed that this process yielded CB nanoparticles with a mean particle size of approximately 200 nm and a dispersity of 0.21 (Figure 1A). Imaging by transmission electron microscopy revealed that the CB nanoparticles were aggregates of even smaller spherules of approximately 25–30 nm in size (Figure 1B, inset). Assuming a spherical shape (with a 200-nm diameter) for the aggregate and a spherical shape (with a 25-nm diameter) for the spherules, we calculated that each aggregate consisted of approximately 133 spherules.

Given our goal of heating particles to generate photoacoustic emissions, nanoparticle size and composition are critically important. Nanoparticle temperature is maximized by preventing heat transfer from the nanoparticle to the surroundings during the laser exposure, so that all heat is retained within the nanoparticle. Minimizing heat loss is achieved by reducing thermal conductivity and surface-to-volume ratio of the nanoparticle. CB has a

relatively low thermal conductivity (e.g., compared with metal nanoparticles) [39], which facilitates heat retention at 200 nm mean diameter. The time scale of thermal conduction to the surroundings is approximately 175 ns (see Supplementary Data), which is much slower than heat deposition time scale of the laser pulse (i.e., 5–9 ns). In contrast, the time scale of heat loss to the surroundings for a 50-nm diameter nanoparticle is approximately 11 ns (see Supplementary Data), which is similar to the laser pulse length, suggesting that a 50-nm nanoparticle is too small, because it would lose heat to its surroundings during the pulse. Moreover, as nanoparticle size decreases, the melting point of CB decreases as well [41], which further motivated us to avoid making nanoparticles too small. We therefore concluded that nanoparticles on the order of 200 nm in size would be effective for our application. Although polydisperse, the majority of nanoparticles used in this study was approximately of that size (modal hydrodynamic diameter ~ 200 nm), and very few were as small as 50 nm (Figure 1A).

We finally tested the acoustic output of the CB nanoparticle suspension when subjected to laser irradiation. To do so, CB suspensions were exposed to pulsed nanosecond lasers and pressure signals were detected using a hydrophone. CB suspensions exposed to 100 mJ/cm^2 produced a peak pressure of 0.17 MPa measured at a distance of 5 mm from the CB suspension (Figure 1B); the pressure within the CB suspension was probably significantly higher. The pressure wave was characterized by an initial delay, which can be attributed to the time for the acoustic wave to reach the detector from the source (i.e., t = d/c = (0.005 m)/(1491 m/s) = 3.35 e–06 s, where t is time delay, d is distance between the CB nanoparticle suspension and hydrophone and c is the speed of sound in water at 23°C) [42], followed by a sudden rise of pressure within 100 ns, followed by a slower recovery within 1 μs. The whole event from pressure rise to negligible signal lasts less than 1 μs, which suggests that the sound generation was due to an expansion-type mechanism involving thermal expansion of CB nanoparticles themselves or expansion of vapor/gas bubbles produced by heat transfer from the hot CB nanoparticles [27]. The frequency spectrum showed a broad range of signals from a few kHz up to 30 MHz, beyond which the signal became largely indistinguishable from background noise. When fluence was increased, the peak pressure likewise increased (Figure 1C), which is expected because greater fluence should cause greater heating of the CB nanoparticle which should cause greater thermal expansion of the CB nanoparticles and its surrounding vapor/ gas shell. The relatively small error bars indicate that the output pressure was consistent from pulse to pulse. Overall, these studies show that the CB nanoparticles and laser irradiation conditions used in this study are capable of generating photoacoustic outputs.

Intracellular drug delivery with laser-activated CB nanoparticles

To address our long-term goal of treating ovarian cancer by intracellular delivery of siRNA, we next identified conditions that enable efficient delivery of molecules into ovarian cancer cells guided by prior literature [31]. Human ovarian cancer cells (HeyA8-F8) were mixed with CB nanoparticles and 70-kDa FITC-dextran (molecular diameter, ~ 6 nm [43]), which was used as a surrogate for the 13-kDa siRNA used in this study (molecular size, ~ 5.6 × ~ 2.6 nm [44]); exposed to laser; washed by centrifugation and then imaged by fluorescence microscopy and analyzed quantitatively by flow cytometry (Figure 2).

Microscopic imaging revealed that laser-irradiation with CB nanoparticles induced uptake of FITC-dextran (as indicated by the green cells) and decreased cell viability (as indicated by the red cells) (Figure 2A). Flow cytometry analysis provided quantitative data (Figure 2B). In control experiments using untreated cells (i.e., cells with no FITC-dextran, no CB nanoparticles and no laser irradiation) or sham-treated cells (i.e., cells with FITC-dextran and CB nanoparticles, but no laser irradiation), there was high viability and negligible uptake.

In flow cytometry analysis, cells were identified based on light scattering (population P1 on graphs of SSC-A vs FSC-A) (Figure 2C). Cells with intracellular uptake of FITC-dextran were identified by green fluorescence (population P4 with elevated fluorescence on FITC-A histograms) (Figure 2C) among those events classified as cells (population P1) and excluding those classified as nonviable (population P3).

Loss of cell viability was determined by two methods. First, nonviable, intact cells were identified by red-fluorescent propidium iodide staining (elevated fluorescence on the PerCP-Cy5–5-A histograms) (Figure 2C). To account for cells fragmented into small pieces that would appear as variable numbers of events with low light scatter (i.e., gated out on graphs of SSC-A vs FSC-A) (Figure 2C), we determined the concentration of intact cells (population P1) in each sample based on the flow rate through the flow cytometer and, by mass balance, calculated the number of cells ‘lost’ in the process, as described previously [45]. In the example shown in Figure 2C, just 6% of cells were identified as nonviable based on propidium iodide staining, whereas another 40% of cells were identified as fragmented based on the mass balance calculation. This shows that a large fraction of cell death can be due to cell fragmentation. Viability data are reported in this study based on the sum of both types of cell viability loss. In this study, we were concerned with immediate effects of the NIR laser and CB interaction on the cells. Therefore, the viability of cells was quantified immediately after cell exposure by propidium iodide staining. As an initial assessment of the long-term effects of laser-CB interaction, we also imaged cultured cells 24 h after laser exposure (Supplementary Figure 2).

We next exposed cells to three different laser-irradiation conditions, which were selected because they had previously been shown to drive intracellular uptake into another cell line – DU145 prostate cancer cells [31] and we therefore expected them to be similarly effective in the ovarian cancer cells used in this study. At each of these three laser irradiation conditions, there was significant uptake of FITC-dextran (2-tailed t-test with Welch’s correction; $p < 0.05$) with associated loss of viability (2-tailed t-test with Welch’s correction; $p < 0.05$). More specifically, all three laser-irradiation conditions led to similar effects: uptake seen in about half of the cells and loss of viability in about one-third of the cells (Figure 2B). These results are similar to those seen with the prostate cancer cells previously [31].

Closer examination of the flow cytometry data allowed us to assess the relative intracellular concentration of FITC-dextran taken up into the cells. The representative histogram plots (Figure 2D) show the levels of green fluorescence among the viable cells in each sample. In graph i, background fluorescence is shown. In graph ii, heterogeneous uptake is seen, with most cells exhibiting significant uptake (i.e., high uptake cells) and a fraction of cells with

low signal (low/no uptake cells). In graph iii, a larger fraction of the cells exhibits high uptake and, finally, in graph iv almost all cells exhibit high uptake. Note that these data only include viable cells and do not account for fragmented cells. Cells fragmented during the laser exposure are accounted for in Figure 2B.

These data are interesting because they suggest a threshold phenomenon, where cells either have high uptake (i.e., the population of cells on the right side of each graph) or they have low/no uptake (i.e., the population of cells on the left side of each graph). We do not see a broad distribution of uptake levels in these graphs. This finding is consistent with previous observations in the context of intracellular delivery by acoustic cavitation and by electroporation [46,47].

The three laser-irradiation conditions shown in Figure 2B have increasing laser fluence that is compensated for by decreasing irradiation time to keep the total fraction of cells affected by the exposure approximately constant (i.e., the sum of cells with intracellular uptake and nonviable cells). However, at higher laser fluence, there were more cells with high uptake (Figure 2D). Combined, these observations suggest that at the three conditions studied, the same fraction of cells experienced permeabilizing effects of laser-activated CB nanoparticles, but the degree of permeabilization experienced by each individual cell was greater at higher laser fluence, resulting in more molecules delivered into each affected cell.

siRNA delivery & knockdown

The next step was to assess intracellular delivery of anti-*EGFR* siRNA to see the siRNA uptake and knockdown of target *EGFR* gene. Anti-*EGFR* siRNA or a negative-control (NC) siRNA were added to ovarian cancer cell suspensions with 25 mg/l CB nanoparticles and the samples were either laser-irradiated (19 mJ/cm^2 for 7 min) or not exposed to laser (sham). Some samples were alternatively exposed to laser without the presence of CB nanoparticles. After 24 h postexposure incubation, cellular RNA was isolated and then analyzed for siRNA uptake and for *EGFR* knockdown by quantitative PCR (qPCR) assays. Intracellular GAPDH was used as an internal control against which *EGFR* mRNA levels were normalized.

To assess siRNA uptake, cells were laser-irradiated in the presence of anti-*EGFR* siRNA with CB nanoparticles (experimental group, 1), anti-*EGFR* siRNA without CB nanoparticles (negative control, 2) or NC siRNA with CB nanoparticles (negative control, 3). The overall difference among 3 experimental conditions (1, 2 and 3) is statistically significant (ANOVA, $p < 0.001$). There was no statistical difference (post-test, $p > 0.05$) in normalized anti-*EGFR* siRNA signal between the two negative controls (Figure 3A). However, there was significantly higher anti-*EGFR* siRNA signal in the experimental group (post-test, $p < 0.001$) compared with either of the negative controls. The fold change of normalized anti-*EGFR* siRNA signal of the experimental group compared with the no-CB negative control was approximately 12,000 and compared with the NC siRNA negative control was approximately 360. Although no *EGFR* siRNA was present in the NC siRNA negative control experiment, there was nonetheless a signal for *EGFR* siRNA detected in the assay. However, this signal is much weaker relative to the signal displayed by *EGFR* siRNA-transfected cells and likely results from nonspecific changes induced by transfection of cells

with NC siRNA. Even weaker *EGFR* siRNA signal was detected in cells treated with *EGFR* siRNA and IR in the absence of CB particles.

As a positive control, we delivered anti-*EGFR* siRNA to ovarian cancer cells using a commercial transfection reagent, Lipofectamine 2000. This delivery method also showed significantly higher intracellular delivery of anti-*EGFR* siRNA compared with NC siRNA negative control (Supplementary Figure 3A) and significantly decreased expression of target *EGFR* gene compared with NC siRNA negative control (Supplementary Figure 3B), which provides a further validation of the siRNA quality and qPCR assay employed in our experiments. It should be noted, that in this study we are not directly comparing our method to the lipid based delivery in terms of efficacy but we use it as a way to validate our experimental methods. Our results also demonstrate that the presence of CB particles is necessary for the transfection to occur and that CB alone without laser-irradiation and anti-*EGFR* siRNA does not affect the expression of *EGFR* gene in treated cells (Supplementary Figure 4). While delivery using this lipid-based method was effective, our photoacoustic approach has the advantage of potential use *in vivo*, whereas Lipofectamine 2000 is recommended only for *in vitro* use [48].

Visual inspection of cells 24 h post-treatment (Supplementary Figure 2) revealed confluence in the no-CB negative control samples, but there was lesser cell density in the experimental group and NC siRNA negative control samples both of which were exposed to laser irradiation in the presence of CB nanoparticles, indicating some loss of cell viability consistent with the dextran-uptake experiments (Figure 2B).

Encouraged by evidence of intracellular delivery of siRNA, we finally assessed knockdown of *EGFR* mRNA compared with the negative control that was laser-irradiated with CB nanoparticles and NC siRNA. The mean expression of the target *EGFR* gene was knocked down by approximately 49% compared with the negative control (2-tailed t-test with Welch's correction, $p < 0.05$). There was also knockdown of *EGFR* mRNA in positive control cells exposed to anti-*EGFR* siRNA with Lipofectamine 2000 (Supplementary Figure 3B), which is consistent with the central question of this study concerning the ability of our photoacoustic method to deliver siRNA into ovarian cancer cells to knock down expression of its target gene.

Fifty-four percent of cells took up dextran at the conditions used in the siRNA experiment (Figure 2B). If we assume that a similar percentage of cells took up siRNA (which may be an underestimate given somewhat larger size of the dextran used in this study compared with the siRNA) and we assume that *EGFR* expression was knocked down by 100% in each affected cell, then 49% knockdown of *EGFR* mRNA (Figure 3B) corresponds to approximately 90% of cells with siRNA uptake (i.e., 49%/54% = 91%). If we instead assume that cells with siRNA uptake exhibited some residual level of *EGFR* expression (less than 100% *EGFR* knockdown), then the percentage of cells with siRNA uptake would be higher than 91%. While this analysis is rough and based on assumptions, our data nonetheless suggest that most cells that had siRNA uptake had significant knockdown. This indicates not only that our photoacoustic method efficiently delivered siRNA into ovarian cancer cells, but that functionally intact siRNA was delivered, and it was delivered into the

correct cellular compartment (i.e., cytosol) that allowed it to silence expression of its target gene. Further optimization of laser exposure parameters, CB nanoparticle concentration and other experimental conditions could lead to more efficient siRNA delivery and gene-expression knockdown (e.g., careful optimization of conditions led to intracellular delivery into ~ 90% of DU145 human prostate cancer cells while maintaining essentially full cell viability [30,31]).

Conclusion

This study shows that laser-activated CB nanoparticles enabled intracellular delivery of siRNA and knockdown of its target *EGFR* mRNA. Initial experiments showed that CB nanoparticles generated photoacoustic emission upon NIR irradiation and intracellular delivery of dextran molecules into viable cells. Photoacoustic delivery of siRNA into ovarian cancer cells resulted in 12,000 times higher normalized *EGFR* siRNA signal compared with negative control cells, indicating dramatically increased uptake of siRNA molecules. This led to statistically significant 49% knockdown of *EGFR* expression on mRNA level. We conclude that delivery of siRNA to ovarian cancer cells using laser-activated carbon nanoparticles is a promising method of intracellular delivery with future possible uses in siRNA-based treatments. Future experiments will require additional delivery optimization, as well as translation into the complex environment of ovarian cancer tumors *in vivo*.

Future perspective

This study presents a novel method to deliver naked siRNA molecules into cells. This delivery is believed to occur by transport through transiently induced transmembrane pores. The method has potential to reduce the risk of endosomal entrapment and degradation of siRNA often associated with other methods of siRNA delivery. In addition, this method of siRNA delivery has the potential to target tumor cells by tumor site-specific laser irradiation and tumor tissue-specific accumulation of CB nanoparticles via the enhanced permeability and retention effect. With further development, delivery of siRNA to ovarian cancer cells using laser-activated carbon nanoparticles could provide a powerful approach to targeted cancer therapy using siRNA.

Supplementary Material

Refer to Web version on PubMed Central for supplementary material.

Acknowledgments

The authors thank P Chakravarty and M Gray for providing us with TEM images and acoustic data, respectively, and L Wang for transfecting HeyA8 cell line. The authors would like to thank D Bondy for providing administrative support.

References

Papers of special note have been highlighted as:

• of interest

1. Fire A, Xu S, Montgomery MK, Kostas SA, Driver SE, Mello CC. Potent and specific genetic interference by double-stranded RNA in *Caenorhabditis elegans*. Nature. 1998; 391(6669):806–811. [PubMed: 9486653]
2. Elbashir SM, Harborth J, Lendeckel W, Yalcin A, Weber K, Tuschl T. Duplexes of 21-nucleotide RNAs mediate RNA interference in cultured mammalian cells. Nature. 2001; 411(6836):494–498. [PubMed: 11373684]
3•. Whitehead KA, Langer R, Anderson DG. Knocking down barriers: advances in siRNA delivery. Nat Rev Drug Discov. 2009; 8(2):129–138. The authors provide an update on the progress of RNAi therapeutics and highlight novel synthetic materials for the encapsulation and intracellular delivery of nucleic acids. They also talk about therapeutic application of siRNA in the clinical setting and ongoing clinical trials. [PubMed: 19180106]
4. Frank-Kamenetsky M, Grefhorst A, Anderson NN, et al. Therapeutic RNAi targeting PCSK9 acutely lowers plasma cholesterol in rodents and LDL cholesterol in nonhuman primates. Proc Natl Acad Sci USA. 2008; 105(33):11915–11920. [PubMed: 18695239]
5. Sato Y, Murase K, Kato J, et al. Resolution of liver cirrhosis using vitamin A-coupled liposomes to deliver siRNA against a collagen-specific chaperone. Nat Biotechnol. 2008; 26(4):431–442. [PubMed: 18376398]
6. Song E, Lee SK, Wang J, et al. RNA interference targeting Fas protects mice from fulminant hepatitis. Nat Med. 2003; 9(3):347–351. [PubMed: 12579197]
7. Morrissey DV, Lockridge JA, Shaw L, et al. Potent and persistent *in vivo* anti-HBV activity of chemically modified siRNAs. Nat Biotechnol. 2005; 23(8):1002–1007. [PubMed: 16041363]
8. Niu XY, Peng ZL, Duan WQ, Wang H, Wang P. Inhibition of HPV 16 E6 oncogene expression by RNA interference *in vitro* and *in vivo*. Int J Gynecol Cancer. 2006; 16(2):743–751. [PubMed: 16681755]
9. Takeshita F, Minakuchi Y, Nagahara S, et al. Efficient delivery of small interfering RNA to bone-metastatic tumors by using atelocollagen *in vivo*. Proc Natl Acad Sci USA. 2005; 102(34):12177–12182. [PubMed: 16091473]
10•. Tabernero J, Shapiro GI, Lorusso PM, et al. First-in-humans trial of an RNA interference therapeutic targeting VEGF and KSP in cancer patients with liver involvement. Cancer Discov. 2013; 3(4):406–417. The findings in this report show safety, pharmacokinetics, RNAi mechanism of action and clinical activity with a novel first-in-class LNP-formulated RNAi therapeutic in patients with cancer. [PubMed: 23358650]
11. Davis ME. The first targeted delivery of siRNA in humans via a self-assembling, cyclodextrin polymer-based nanoparticle: from concept to clinic. Mol Pharmaceut. 2009; 6(3):659–668.
12. Shegokar R, Al Shaal L, Mishra PR. SiRNA delivery: challenges and role of carrier systems. Pharmazie. 2011; 66(5):313–318. [PubMed: 21699063]
13. Tomar RS, Matta H, Chaudhary PM. Use of adeno-associated viral vector for delivery of small interfering RNA. Oncogene. 2003; 22(36):5712–5715. [PubMed: 12944921]
14. Devroe E, Silver PA. Retrovirus-delivered siRNA. BMC Biotechnol. 2002; 2:15. [PubMed: 12199908]
15. Hughes J, Yadava P, Mesaros R. Liposomal siRNA delivery. Methods Mol Biol. 2010; 605:445–459. [PubMed: 20072900]
16. Podesta JE, Kostarelos K. Chapter 17 – engineering cationic liposome siRNA complexes for *in vitro* and *in vivo* delivery. Methods Enzymol. 2009; 464:343–354. [PubMed: 19903563]
17. Rosi NL, Giljohann DA, Thaxton CS, Lytton-Jean AK, Han MS, Mirkin CA. Oligonucleotide-modified gold nanoparticles for intracellular gene regulation. Science. 2006; 312(5776):1027–1030. [PubMed: 16709779]
18. Giljohann DA, Seferos DS, Prigodich AE, Patel PC, Mirkin CA. Gene regulation with polyvalent siRNA-nanoparticle conjugates. J Am Chem Soc. 2009; 131(6):2072–2073. [PubMed: 19170493]
19. Davis ME, Zuckerman JE, Choi CH, et al. Evidence of RNAi in humans from systemically administered siRNA via targeted nanoparticles. Nature. 2010; 464(7291):1067–1070. [PubMed: 20305636]
20. Lewis DL, Wolff JA. Systemic siRNA delivery via hydrodynamic intravascular injection. Adv Drug Deliv Rev. 2007; 59(2–3):115–123. [PubMed: 17442446]

21. Thomas CE, Ehrhardt A, Kay MA. Progress and problems with the use of viral vectors for gene therapy. Nat Rev Genet. 2003; 4(5):346–358. [PubMed: 12728277]
22. Howard DB, Powers K, Wang Y, Harvey BK. Tropism and toxicity of adeno-associated viral vector serotypes 1, 2, 5, 6, 7, 8, and 9 in rat neurons and glia *in vitro*. Virology. 2008; 372(1):24–34. [PubMed: 18035387]
23. DE Bruin KG, Fella C, Ogris M, Wagner E, Ruthardt N, Brauchle C. Dynamics of photoinduced endosomal release of polyplexes. J Control Release. 2008; 130(2):175–182. [PubMed: 18585413]
24. Mintzer MA, Simanek EE. Nonviral vectors for gene delivery. Chem Rev. 2009; 109(2):259–302. [PubMed: 19053809]
25. Oishi M, Kataoka K, Nagasaki Y. pH-responsive three-layered PEGylated polyplex micelle based on a lactosylated ABC triblock copolymer as a targetable and endosome-disruptive nonviral gene vector. Bioconjug Chem. 2006; 17(3):677–688. [PubMed: 16704205]
26. Rodriguez-Devora JI, Ambure S, Shi ZD, Yuan Y, Sun W, Xui T. Physically facilitating drug-delivery systems. Ther Deliv. 2012; 3(1):125–139. [PubMed: 22485192]
27. Park HK, Kim D, Grigoropoulos CP, Tam AC. Pressure generation and measurement in the rapid vaporization of water on a pulsed-laser-heated surface. J Appl Phys. 1996; 80(7):4072–4081.
28. Kitz M, Preisser S, Wetterwald A, Jaeger M, Thalmann GN, Frenz M. Vapor bubble generation around gold nanoparticles and its application to damaging of cells. Biomed Opt Express. 2011; 2(2):291–304. [PubMed: 21339875]
29•. Chen H, Diebold G. Chemical generation of acoustic waves: a giant photoacoustic effect. Science. 1995; 270(5238):963–966. Presents the first demonstration to show that acoustic waves are emitted when carbon black solutions are exposed to near-infrared laser.
30•. Chakravarty P, Qian W, El-Sayed MA, Prausnitz MR. Delivery of molecules into cells using carbon nanoparticles activated by femtosecond laser pulses. Nat Nanotechnol. 2010; 5(8):607–611. Demonstrates efficient uptake of molecules into mammalian cells for the first time using femtosecond laser pulses and carbon black nanoparticles. [PubMed: 20639882]
31•. Sengupta A, Kelly SC, Dwivedi N, Thadhani N, Prausnitz MR. Efficient intracellular delivery of molecules with high cell viability using nanosecond-pulsed laser-activated carbon nanoparticles. ACS Nano. 2014; 8(3):2889–2899. Demonstrates intracellular uptake of calcein and dextran using a cost-effective nanosecond laser. The study also shows the effect of various parameters that affect the final delivery efficiency. [PubMed: 24547946]
32•. Huang X, Pallaoro A, Braun GB, et al. Modular plasmonic nanocarriers for efficient and targeted delivery of cancer-therapeutic siRNA. Nano Lett. 2014; 14(4):2046–2051. Shows that delivery of siRNA is achieved when siRNA is released from gold nanoshells when exposed to pulsed laser. [PubMed: 24597503]
33. Siegel R, Naishadham D, Jemal A. Cancer statistics, 2012. CA Cancer J Clin. 2012; 62(1):10–29. [PubMed: 22237781]
34. Institute Nc. http://seer.cancer.gov/statfacts/html/ovary.html
35. Ozols RF. Treatment goals in ovarian cancer. Int J Gynecol Cancer. 2005; 15(Suppl 1):3–11. [PubMed: 15839952]
36. Dickerson EB, Blackburn WH, Smith MH, Kapa LB, Lyon LA, McDonald JF. Chemosensitization of cancer cells by siRNA using targeted nanogel delivery. BMC Cancer. 2010; 10:10. [PubMed: 20064265]
37. Weissleder R. A clearer vision for *in vivo* imaging. Nat Biotechnol. 2001; 19(4):316–317. [PubMed: 11283581]
38. Stolik S, Delgado Ja, Pérez A, Anasagasti L. Measurement of the penetration depths of red and near infrared light in human *"ex vivo"* tissues. J Photochem Photobiol B. 2000; 57(2–3):90–93. [PubMed: 11154088]
39. Han D, Meng Z, Wu D, Zhang C, Zhu H. Thermal properties of carbon black aqueous nanofluids for solar absorption. Nanoscale Res Lett. 2011; 6:457. [PubMed: 21767359]
40. Fang J, Nakamura H, Maeda H. The EPR effect: unique features of tumor blood vessels for drug delivery, factors involved, and limitations and augmentation of the effect. Adv Drug Deliv Rev. 2011; 63(3):136–151. [PubMed: 20441782]

41. Roduner E. Size matters: why nanomaterials are different. Chem Soc Rev. 2006; 35(7):583–592. [PubMed: 16791330]
42. Lubbers J, Graaff R. A simple and accurate formula for the sound velocity in water. Ultrasound Med Biol. 1998; 24(7):1065–1068. [PubMed: 9809641]
43. Armstrong JK, Wenby RB, Meiselman HJ, Fisher TC. The hydrodynamic radii of macromolecules and their effect on red blood cell aggregation. Biophys J. 2004; 87(6):4259–4270. [PubMed: 15361408]
44. Liu H, Li Y, Mozhi A, et al. siRNA-phospholipid conjugates for gene and drug delivery in cancer treatment. Biomaterials. 2014; 35(24):6519–6533. [PubMed: 24797882]
45. Hallow DM, Mahajan AD, Mccutchen TE, Prausnitz MR. Measurement and correlation of acoustic cavitation with cellular bioeffects. Ultrasound Med Biol. 2006; 32(7):1111–1122. [PubMed: 16829325]
46. Canatella PJ, Karr JF, Petros JA, Prausnitz MR. Quantitative study of electroporation-mediated molecular uptake and cell viability. Biophys J. 2001; 80(2):755–764. [PubMed: 11159443]
47. Guzman HR, Nguyen DX, Khan S, Prausnitz MR. Ultrasound-mediated disruption of cell membranes. I Quantification of molecular uptake and cell viability. J Acoust Soc Am. 2001; 110(1):588–596. [PubMed: 11508983]
48. Dalby B, Cates S, Harris A, et al. Advanced transfection with Lipofectamine 2000 reagent: primary neurons, siRNA, and high-throughput applications. Methods. 2004; 33(2):95–103. [PubMed: 15121163]

Executive summary

- Delivery of siRNA into cells is a challenging task and mostly limited to viral vectors, lipid vesicles and solid nanoparticle formulations.
- This study explores an alternative technique of siRNA delivery into cells using laser-activated carbon black (CB) nanoparticles.
- The method involves exposure of CB nanoparticles to nanosecond pulsed laser, causing the nanoparticles to preferentially heat up, which results in particle expansion, liquid vaporization and/or chemical reaction, followed by generation of acoustic waves, leading to poration of cell membranes. Molecules then passively transport into the cell without the need of endocytosis.
- The method was previously demonstrated to be efficient in delivering small molecules into cells and in this study the technique is being expanded into delivering siRNA.

Delivery system design

- There are three main components to the current system viz: the laser, the CB nanoparticles and the siRNA to be delivered.
- A Nd:YAG nanosecond laser (5–9 ns) with a 1064-nm wavelength was chosen because it has a deeper penetration into the tissue than lower wavelength light and is very efficiently absorbed by CB.
- CB nanoparticles were prepared by sonicating CB in water with a stabilizer at a final concentration of 400 mg/l with a mean size of approximately 200 nm. Acoustic wave generation was observed and measured when CB nanoparticles were exposed to laser pulses.
- siRNA chosen for the study was an anti-*EGFR* siRNA which has the potential to treat ovarian and other cancers.

Intracellular drug delivery with laser-activated CB nanoparticles

- Preliminary demonstration of uptake was shown using 70-kDa FITC dextran using ovarian cancer cells (HeyA8-F8) as the target.
- Microscopic imaging and flow cytometric analysis revealed that laser-rradiation with CB nanoparticles induced uptake of FITC-dextran and to some extent decreased the cell viability.

siRNA delivery & knockdown

- To assess the delivery efficiency of siRNA, two tests were conducted: total anti-*EGFR* siRNA was quantified to assess the uptake, and the *EGFR* mRNA levels were quantified using qPCR to assess the knockdown.
- When cells were exposed at 19 mJ/cm^2 for 7 min, the siRNA levels (normalized anti-*EGFR* siRNA signal) in the exposed cells were about 12,000 times higher

compared with negative control cells leading to a 49% knockdown of *EGFR* expression as assessed on the mRNA level.

Conclusion

- This study shows for the first time that laser-activated CB nanoparticles enabled intracellular delivery of siRNA and knockdown of its target *EGFR* mRNA.
- Future experiments will require additional delivery optimization, as well as translation into the complex environment of ovarian cancer tumors *in vivo*.

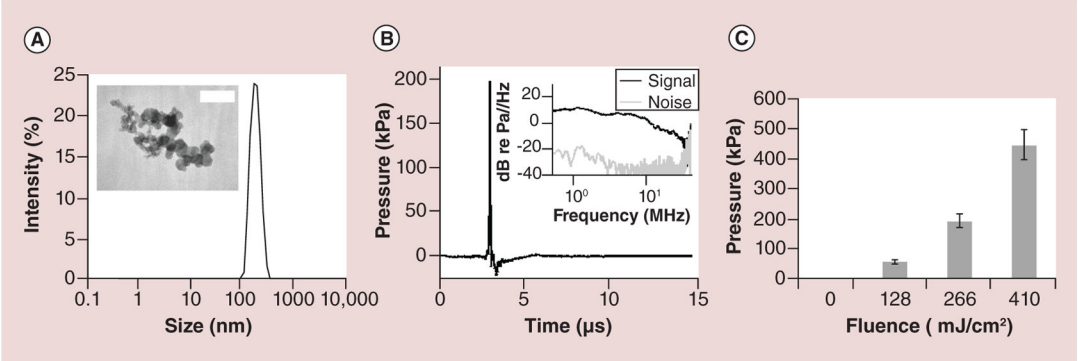

Figure 1. Physical characterization of carbon black nanoparticles

(A) Representative dynamic light scattering measurement of hydrodynamic diameter of carbon black (CB) nanoparticle aggregates in DI water suspension at a final concentration of 25 μg/l shows a single peak and no particle settling. Transmission electron microscope image (inset) of dried CB nanoparticle aggregates shows the individual spherules constituting the aggregates. The scale bar is 50 nm. **(B)** Representative acoustic output (pressure) vs time measured using a hydrophone when CB nanoparticle suspension (50 mg/l) was exposed to a single laser pulse at 250 mJ/cm^2 fluence. The frequency distribution calculated from the hydrophone calibration curve reveals a broadband signal up to approximately 30 MHz (inset). **(C)** Peak acoustic pressure shown as a function of laser fluence. Peak pressure increased with increasing fluence. Data show mean ± standard deviation with more than 100 replicates each (n > 100).

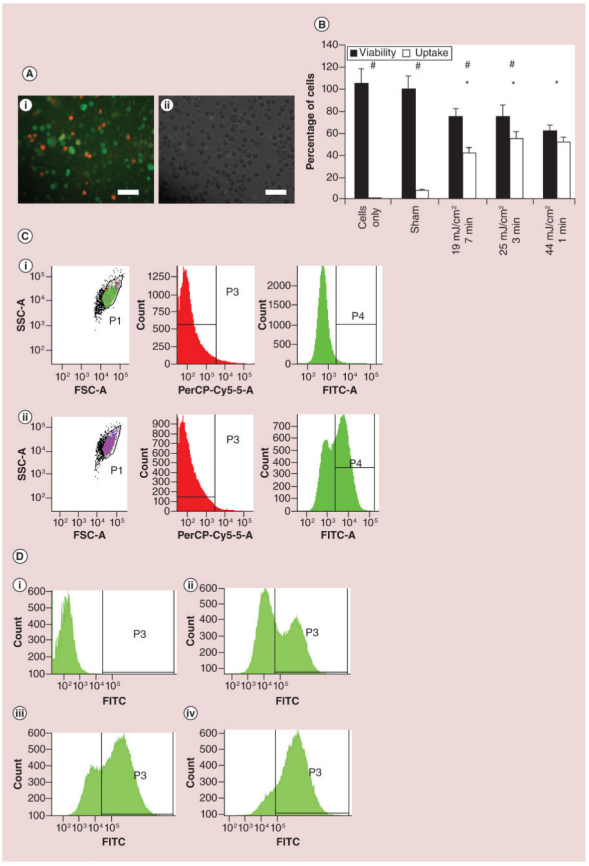

Figure 2. Intracellular delivery of FITC-dextran in HeyA8-F8 ovarian cancer cells (see facing page)

(A) Cells inspected by microscopic imaging show uptake of 70-kDa FITC-conjugated dextran (green) when cells were exposed to laser at 44 mJ/cm^2 for 1 min in the presence of 25 mg/l CB nanoparticles. Cells were also stained with propidium iodide (red), which is a marker of nonviable cells: **(i)** fluorescence microscopy, and **(ii)** brightfield microscopy. Scale bars: 100 μm. **(B)** Flow cytometric analysis of percentage of cells remaining viable and exhibiting intracellular uptake of dextran is shown as a function of photoacoustic exposure conditions, including laser fluence (mJ/cm^2) and exposure time (min). The asterisk symbol (*) represents statistically significantly different viability compared to sham samples ($p < 0.05$) for viability compared to sham samples and the hash symbol (#) signifies that percentage of cells with uptake and viability for a given sample is significantly different ($p < 0.05$). Data show mean ± standard deviation (n = 3). **(C)** Representative flow cytometry data: forward scatter (FSC-A) vs side scatter (SSC-A) and histograms of propidium iodide fluorescence (PerCP-Cy5–5-A) and FITC-dextran fluorescence (FITC-A). The upper graphs **(i)** show data after sham treatment of cells. The lower graphs **(ii)** are for samples exposed to 25 mJ/cm^2 for 3 min. **(D)** Representative flow cytometry histogram plots of FITC-dextran fluorescence are shown for cells incubated with FITC-dextran at four conditions shown in **(B): (i)** untreated cells (no laser, no CB nanoparticles), and cells exposed to CB nanoparticles and laser at **(ii)** 19 mJ/cm^2, 7 min **(iii)** 25 mJ/cm^2, 3 min, **(iv)** 44 mJ/cm^2, 1 min.

FITC: Fluorescein isothiocyanate; FSC: Forward scatter; SSC: Side scatter.

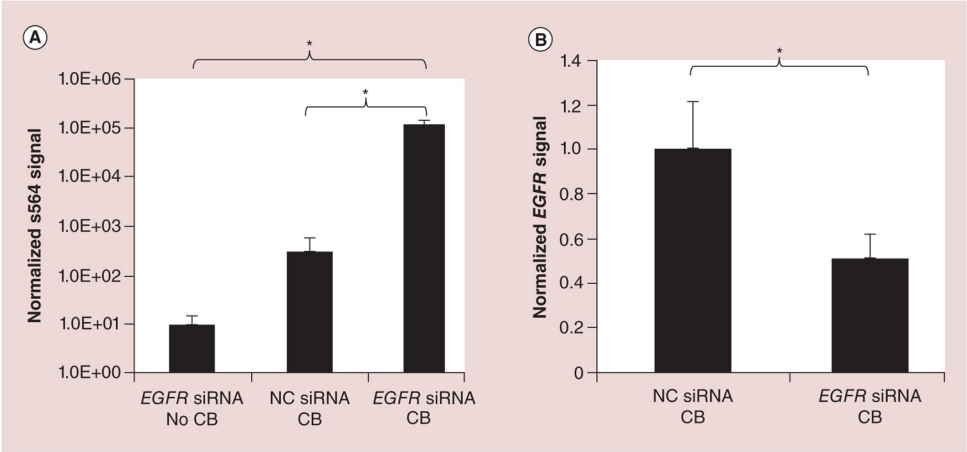

Figure 3. Uptake of anti-*EGFR* siRNA (s564, Life Technologies) and knockdown efficiency of *EGFR* mRNA after photoacoustic delivery in ovarian cancer cells

(A) Amount of intracellular siRNA (s564; in arbitrary units) normalized per 10 ng of total RNA, quantified using quantitative PCR, when HeyA8-F8 cells treated with anti-*EGFR* siRNA or NC siRNA were exposed to laser at 19 mJ/cm^2 for 7 min in the presence (CB) or absence (no CB) of 25 mg/l CB nanoparticles. **(B)** *EGFR* mRNA level normalized relative to GAPDH (quantitative PCR) showing knockdown in cells treated with anti-*EGFR* siRNA exposed to laser with CB nanoparticles (compared NC siRNA).

*Statistically significant differences in uptake and knockdown ($p < 0.05$). Data shown as mean ± standard deviation ($n = 3$).

CB: Carbon black; NC: Negative control.